Nonclassic Evolution of a Cold-Frontal System across the Western United States during the Intermountain Precipitation Experiment (IPEX)

DAVID M. SCHULTZ

Centre for Atmospheric Science, Department of Earth and Environmental Sciences, and Centre for Crisis Studies and Mitigation, University of Manchester, Manchester, United Kingdom

W. JAMES STEENBURGH

Department of Atmospheric Sciences, University of Utah, Salt Lake City, Utah

(Manuscript received 7 August 2019, in final form 26 November 2019)

ABSTRACT

A cold-frontal passage through northern Utah was studied using observations collected during intensive observing period 4 of the Intermountain Precipitation Experiment (IPEX) on 14–15 February 2000. To illustrate some of its nonclassic characteristics, its origins are considered. The front developed following the landfall of two surface features on the Pacific coast (hereafter, the cold-frontal system). The first feature was a surface pressure trough and wind shift associated with a band of precipitation and rope cloud with little, if any, surface baroclinicity. The second, which made landfall 4 h later, was a wind shift associated with weaker precipitation that possessed a weak temperature drop at landfall (1°C in 9 h), but developed a stronger temperature drop as it moved inland over central California (4°–6°C in 9 h). As the first feature moved into the Great Basin, surface temperatures ahead of the trough increased due to downslope flow and daytime heating, whereas temperatures behind the trough decreased as precipitation cooled the near-surface air. Coupled with confluence in the lee of the Sierra Nevada, this trough developed into the principal baroclinic zone of the cold-frontal system (8°C in less than an hour), whereas the temperature drop with the second feature weakened further. The motion of the surface pressure trough was faster than the posttrough surface winds and was tied to the motion of the short-wave trough aloft. This case, along with previously published cases in the Intermountain West, challenges the traditional conceptual model of cold-frontal terminology, structure, and evolution.

1. Introduction

The conventional explanation for the movement of cold fronts is that they move by the advection of postfrontal cold air (e.g., Bjerknes 1919; Sanders 1955; Saucier 1955, p. 270; Wallace and Hobbs 1977, 116–117; Bluestein 1993, p. 259). This explanation works well for many fronts, but there are situations where this does not happen (e.g., Smith and Reeder 1988). One such situation is in regions of complex terrain. Consider a cold front traveling over the Pacific Ocean and making landfall in the western United States. How does such a cold front subsequently pass through the western United States? Is it realistic to expect cold postfrontal air masses to be advected from the Pacific Ocean, across mountain ranges of 2000–3000-m elevation, and through the Intermountain West? Does this postfrontal air mass retain its properties of temperature and moisture throughout its passage across this complex terrain? If the advection of the postfrontal airmass does not control the speed of motion of cold fronts, then the question of what controls frontal movement across the western United States—as well as other locations where complex terrain disrupts the lower-tropospheric frontal structure—becomes a relevant question for synoptic meteorology.

Denotes content that is immediately available upon publication as open access.

Corresponding author: David M. Schultz, david.schultz@manchester.ac.uk

DOI: 10.1175/WAF-D-19-0166.1

Further observations of fronts in the western United States show that they do not match the conventional conceptual model of fronts in the Norwegian cyclone model in other ways, as well. Fronts in the western United States may be associated with weak temperature gradients (Hess and Wagner 1948; McClain and Danielsen 1955), may be modified by the terrain-induced flow (e.g., Steenburgh and Blazek 2001; Neiman et al. 2004; West and Steenburgh 2010), may possess multiple rainbands (e.g., Reynolds and Kuciauskas 1988), may have their thermodynamic structures altered through evaporating precipitation, intense prefrontal surface heating, or orographic effects (e.g., Schultz and Trapp 2003; Shafer and Steenburgh 2008; West and Steenburgh 2010, 2011), or may exhibit discrete propagation (Steenburgh et al. 2009). Indeed, issues with frontal analysis in the western United States were recognized by Williams (1972, p. 1) who identified the "failure of the classical Norwegian frontal model in many cases to adequately portray the synoptic situation as it exists."

In this article, we present a case of a cold-frontal system that crossed the western United States. In describing this case, we were sometimes challenged by what to call features that did not fit the classic conceptual model of a cold front. Consequently, we refer to the entire structure as the *cold-frontal system* to discuss features that do not easily fit into our conceptual models, and we reserve the term *front* for a feature when the temperature gradient associated with a wind shift is quite strong (e.g., Sanders and Doswell 1995; Sanders 1999a).

The goal of this article is to elucidate and explain these nonclassic characteristics and to synthesize across several previously published cases the kinds of processes that affect frontal structure and intensity in the western United States. This event occurred during the field phase of the Intermountain Precipitation Experiment (IPEX), a research program designed to improve the quantitative prediction of precipitation over the Intermountain West of the United States through better understanding of the relevant physical processes (Schultz et al. 2002). Most of the previous research on IPEX was done on the third intensive observing period (IOP 3) where upstream flow blocked along the Wasatch Mountains favored precipitation well away from the slopes (Cox et al. 2005; Colle et al. 2005; Shafer et al. 2006). Also, the first known vertical profiles of the electric field in winter nimbostratus were measured during IOP 3, as well as during other IPEX IOPs (Rust and Trapp 2002). The cold-frontal system studied in the present article was the focus of IPEX's fourth IOP (IOP 4) and was known as the Valentine's Day windstorm. The passage of the front through the Salt Lake Valley was studied by Schultz and Trapp (2003) who described the microscale structure and evolution of the front in northern Utah. They found that subcloud cooling through sublimation and evaporation of precipitation intensified the front and produced a nonclassic, forward-tilting leading edge to the cold advection with height.

In the present article, we investigate the earlier structure and evolution of the cold-frontal system during IPEX IOP 4 from its arrival on the west coast of North America, its eastward movement across the western United States, and through to its arrival in northern Utah. We focus on observational analysis of the data, particularly along the southwest–northeast-oriented cold-frontal system as it moves from the San Francisco Bay Area to northern Utah, where the most interesting evolution occurred and along which the strongest impacts from the front occurred. Section 2 provides a broad perspective on some of the impacts of the frontal system ranging from the western coast of the United States to the Front Range of the Rocky Mountains. Section 3 provides a synoptic overview of the cyclone and its attendant nonfrontal and frontal features on 14–15 February 2000. Section 4 describes the structure of the cold-frontal system during its landfall and passage across California, and section 5 describes its development and evolution over the northern Great Basin and Snake River Plain. Finally, section 6 synthesizes the observations from this case with other previously published cases over the western United States that challenge our conceptual models of cold fronts.

2. Impacts of the cold-frontal system

The 14–15 February 2000 cold-frontal system was associated with a weakening midlatitude cyclone that produced disruptive weather from California to eastern Colorado (Fig. 1). The following reports are a sample of those contained within *Storm Data* (NOAA 2000). A map of station and geographic locations used in this article is found in Fig. 2. Heavy rains and strong winds occurred along the West Coast from southwest Oregon to south of the Bay Area, falling on ground that had already been soaked from several previous days of heavy rain. In Ukiah, California, a tree blew down onto a mobile home, killing the person inside. Along the California coast near the Bay Area, heavy rain, as much as 127 mm (5 in.) in 24 h, led to flash floods and mudslides that closed roads and caused over $5 million (U.S. dollars) in damage (Fig. 1). Highway 1 south of Big Sur was closed for several months due to washouts. Around 42 000 people lost power throughout the Bay Area, with another 2400 people losing power in North Monterey County due

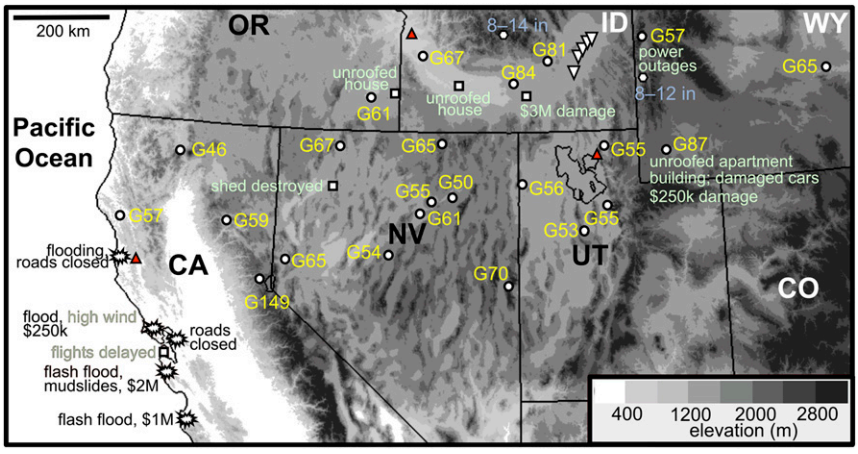

FIG. 1. A selection of *Storm Data* (NOAA 2000) reports for 14 Feb 2000. Wind gusts (kt) are reported in yellow as GXX and are indicated by small white circles. Explosion symbols represent impacts from heavy rain and flooding, squares and green text represent impacts from strong winds, hexagons and blue text represent snowfall amounts (in.), downward-pointing white triangles represent tornadoes, and upward-pointing red triangles represent deaths. Where both wind gusts and descriptions occurred at the same location, a circle was used. Elevation above sea level is shaded every 400 m according to scale.

to fallen trees. Flights were delayed at San Francisco International Airport. The heaviest rain on the coast ended by 1800 UTC 14 December.

Farther east, it was not the heavy precipitation and strong wind, but the strong wind that was the principal concern for forecasters (Fig. 1). Although strong winds accompanied this cyclone, they were often enhanced at the frontal passage. A wind sensor on top of Ward Peak, west of Lake Tahoe, recorded a peak wind gust of $77\,m\,s^{-1}$ (149 kt) (1 kt $\approx 0.51\,m\,s^{-1}$). The Reno NWS Forecast Office reported wind gusts of $33\,m\,s^{-1}$ (65 kt), and the Elko NWS Forecast Office (EKO) reported $28\,m\,s^{-1}$ (63 mph). Other notable wind gusts from Remote Automated Weather Stations (RAWS) sites include Mather, California ($36\,m\,s^{-1}$, 81 mph), and Texas Springs, Nevada ($34\,m\,s^{-1}$, 77 mph).

The winds continued to cause damage in southern Idaho where semi trucks and cars were blown off Interstate 84 and a house in Hagerman lost a roof (Fig. 1). A tree fell onto a car in Nampa, Idaho, and the elderly driver was transported to the hospital where she died of a heart attack. In southeast Idaho, straight-line winds resulted in $3.5 million in damage, with over $1 million to irrigation wheel lines alone. Minidoka, Idaho, recorded state-record gusts to $43.0\,m\,s^{-1}$ (96.3 mph). Power was out at a potato-processing plant and a flour mill, idling over 1000 workers for the next four days. The system spawned an intense band of convection in southeast Idaho that produced two F0 and three F1 tornadoes, the first tornadoes ever reported in Idaho in February (e.g., Schultz et al. 2002, pp. 199–200, 202; LaDue 2002).

In Utah, strong gusts exceeding $26\,m\,s^{-1}$ (50 kt) also occurred (Fig. 2 in Schultz and Trapp 2003). In Brigham City, Utah, a 38-year-old woman was killed on her porch by a falling tree. The strong winds continued into the Front Range of the Rockies with peak gusts exceeding $26\,m\,s^{-1}$ (50 kt) and as high as $36\,m\,s^{-1}$ (70 kt). Two workers were injured in Holyoke, northeast Colorado, when the trusses on which they were standing collapsed in the strong winds. Heavy snow also fell across the

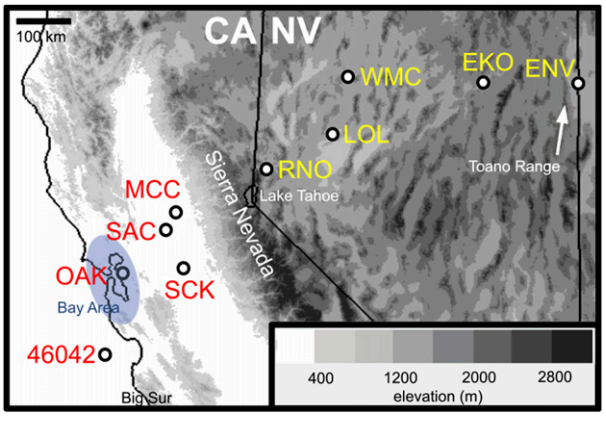

FIG. 2. Station locations in time series plots across California for Fig. 7 (labeled in red) and across Nevada for Fig. 10 (labeled in yellow): buoy 50 km west-northwest of Monterey (46042), Oakland (OAK), McClelland (MCC), Sacramento (SAC), Stockton (SCK), Reno (RNO), Lovelock (LOL), Winnemucca (WMC), Elko (EKO), and Wendover (ENV). Some geographic locations described in text are also labeled. Elevation above sea level is shaded every 400 m according to scale.

West, particularly along the northern part of the system, where up to 38 cm (15 in.) fell in eastern Idaho, western Wyoming, and western Colorado.

In total, the swath of damage from this storm caused three deaths, dozens of injuries, power outages affecting tens of thousands, and over $10 million in damages documented in *Storm Data* alone.

3. Synoptic overview

To provide an overview of this damaging cyclone and attendant cold-frontal system, upper-air maps, infrared satellite imagery, and radar composites for the western United States are presented in this section. We show the temperature field at 700 hPa as an illustration of the synoptic-scale temperature gradient, although temperatures at other lower-tropospheric levels also possess similar structure. At 1200 UTC 14 February 2000, an upper-tropospheric trough lay offshore and was associated with a well-developed midlatitude cyclone (Figs. 3a,c). The 700-hPa warm advection associated with the cyclone brought clouds and precipitation inland over Oregon, southern Washington, southern Idaho, and northern Utah (Figs. 3b,c). Cold advection at 700 hPa remained offshore (Fig. 3b). The precipitation with this event also appears to be associated with upper-level PV advection to the east of the pressure trough (e.g., the dynamic tropopause maps in Fig. 3a) combined with orographic lift. A comma-shaped cloud pattern accompanied the upper-level trough and midlatitude cyclone, with the tail of the comma extending from the cyclone center onshore across Oregon and California ahead of the 700-hPa cold advection. Hereafter, we refer to the tail of this comma as the principal cloud band associated with the cyclone.

By this time, rain had already been falling over California and Oregon for nearly 24 h, which was on top of further heavy rains that had occurred since 10 February. This situation was prone to flooding and landslides, even from a relatively modest plume of moisture associated with this event. The precipitable water from the Rapid Update Cycle had a maximum exceeding 35 mm at 0600 UTC 14 December, but rapidly decreased to 20 mm by 6 h later (not shown). Thus, the precipitation leading up to this frontal passage was associated with a marginal atmospheric river (e.g., Ralph et al. 2004; Rutz et al. 2014).

Within this principal cloud band, heavy orographic precipitation was occurring in the Sierra Nevada of eastern California in the moist (i.e., the near-surface dewpoint in the Oakland, California, sounding at 1200 UTC was 12°C) southwesterly flow (Figs. 3a–c).

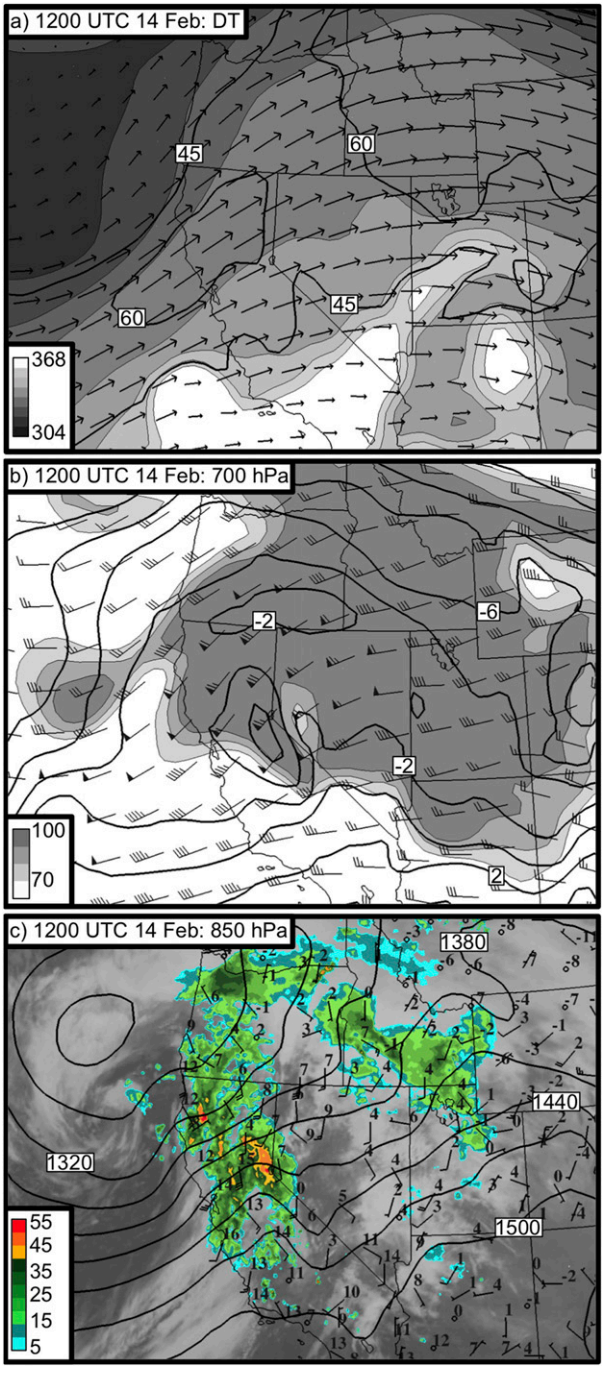

FIG. 3. Regional analyses from the Rapid Update Cycle, version 2 (RUC2; Benjamin et al. 1998) at 1200 UTC 14 Feb 2000. (a) Dynamic tropopause (DT) potential temperature (shaded every 8 K following inset scale), isotachs (contours at 45 and 60 m s^{-1}), and wind vectors. (b) 700-hPa temperatures (contours every 2°C), relative humidity greater than 70% (shaded every 10% following inset scale), and wind (pennants, full barbs, and half-barbs denote 25, 5, and 2.5 m s^{-1}, respectively). (c) 850-hPa geopotential height (contours every 30 m), NEXRAD 8-km composite radar reflectivity (greater than 5 dBZ color-filled following inset scale), infrared satellite imagery, and selected MesoWest surface observations of temperature (°C, upper right) and wind [barbs as in (b)].

For example, the hourly precipitation gauge at Grass Valley Number 2 (732-m elevation; 80 km north-northeast of Sacramento, California) reported 25 mm (1.0 in.) in 4 h (1200–1600 UTC). Despite the heavy precipitation on the windward slopes, radar imagery (Fig. 3c) and hourly precipitation data from stations east of the Sierra Nevada (not shown) indicated little to no measurable precipitation was occurring at this time. Indeed, an unsaturated area at 700 hPa was located just downstream of the Sierra Nevada east of Reno, Nevada, with a lee trough immediately downstream of the southern Sierra Nevada (Figs. 3b,c).

At 1800 UTC, the upper-tropospheric trough approached northern California, and the 850-hPa low moved onshore over Washington and Oregon (Figs. 4a,c). Also, drier tropospheric air from the southwest and descent in the lee of the Sierra cleared out much of the cloudiness over southern California and eastern Nevada (Figs. 4b,c), bringing an end to the heavy precipitation along the coast causing much of the flooding (Fig. 1). This clearing is consistent with 6 h of transport of dry descended air at about 30 m s^{-1} (roughly the 700-hPa wind speed), which moved the edge of the moisture to Utah. Specifically, in 6 h (6 h $\times$ 3600 s h^{-1} $\times$ 30 m s^{-1}), the air would travel 648 km, the approximate distance from the lee of the Sierra (roughly the location of the developing minimum in the moisture at 1200 UTC; Fig. 3b) to the Great Salt Lake (the edge of the moisture at 1800 UTC; Fig. 4b). Troughing at 850 hPa with a coincident band of precipitation developed over northwest Nevada. Confluence in the lee of the Sierra Nevada where southwesterlies in western and northwestern Nevada met with southerlies in southern and eastern Nevada (Fig. 4c) tightened the gradient of isotherms ahead of its prior location, as evidenced by calculations of lower-tropospheric Petterssen (1936) frontogenesis from the Rapid Update Cycle 2 (RUC2; not shown). At this time, the precipitation band, as inferred from radar reflectivity, was strongest from approximately Reno to Winnemucca, Nevada (WMC), but weakened farther north, and the strongest wind gusts occurred at Reno starting at 1730 UTC.

By 2100 UTC, the northern end of the band strengthened and extended to the central Idaho Mountains (Fig. 5a). However, precipitation did not penetrate downstream of the southern Sierra Nevada, typical of eastward-moving cold fronts. By 2300 UTC (Fig. 5b), the northern portion of the band had developed into a tornadic bow echo in southeast Idaho (LaDue 2002; Schultz et al. 2002, their Fig. 10). The event was unusual, being the only cold-season bow echo west of the Rockies in Burke and Schultz's (2004) 4-yr climatology of cold-season bow echoes. Within an hour,

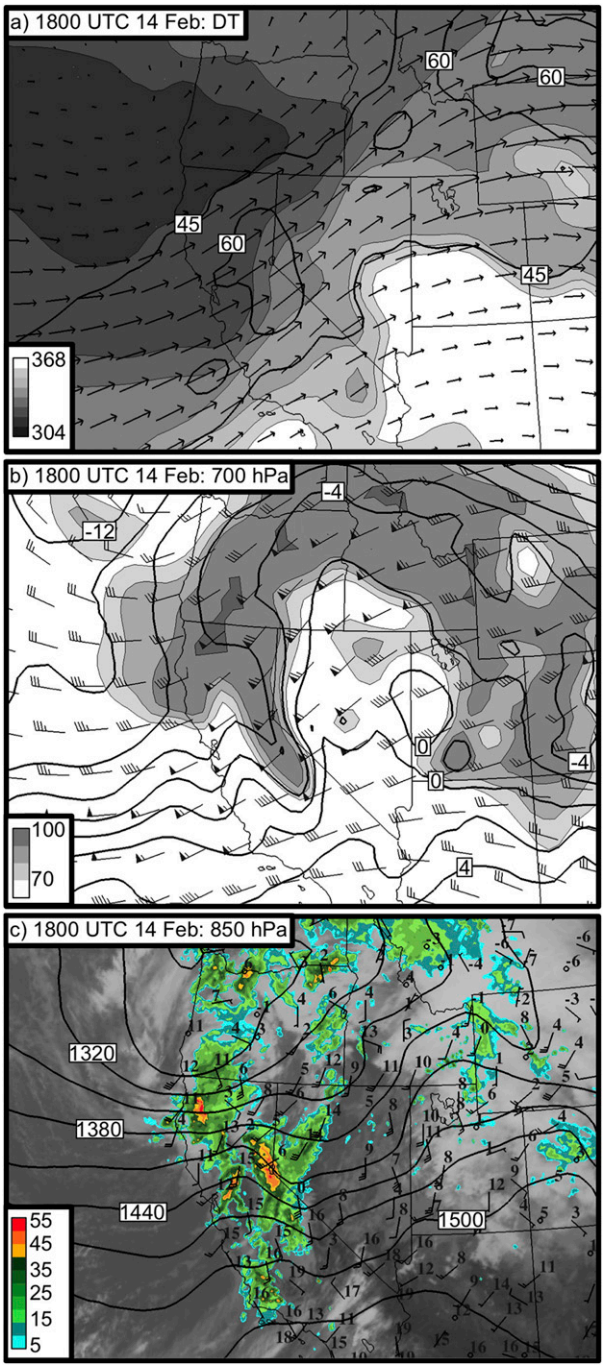

FIG. 4. Regional analyses from the RUC2 at 1800 UTC 14 Feb 2000. (a) Dynamic tropopause (DT) potential temperature (shaded every 8 K following inset scale), isotachs (contours at 45 and 60 m s^{-1}), and wind vectors. (b) 700-hPa temperatures (contours every 2°C), relative humidity greater than 70% (shaded every 10% following inset scale), and wind (pennants, full barbs, and half-barbs denote 25, 5, and 2.5 m s^{-1}, respectively). (c) 850-hPa geopotential height (contours every 30 m), NEXRAD 8-km composite radar reflectivity (greater than 5 dBZ color-filled following inset scale), infrared satellite imagery, and selected MesoWest surface observations of temperature (°C, upper right) and wind [barbs as in (b)].

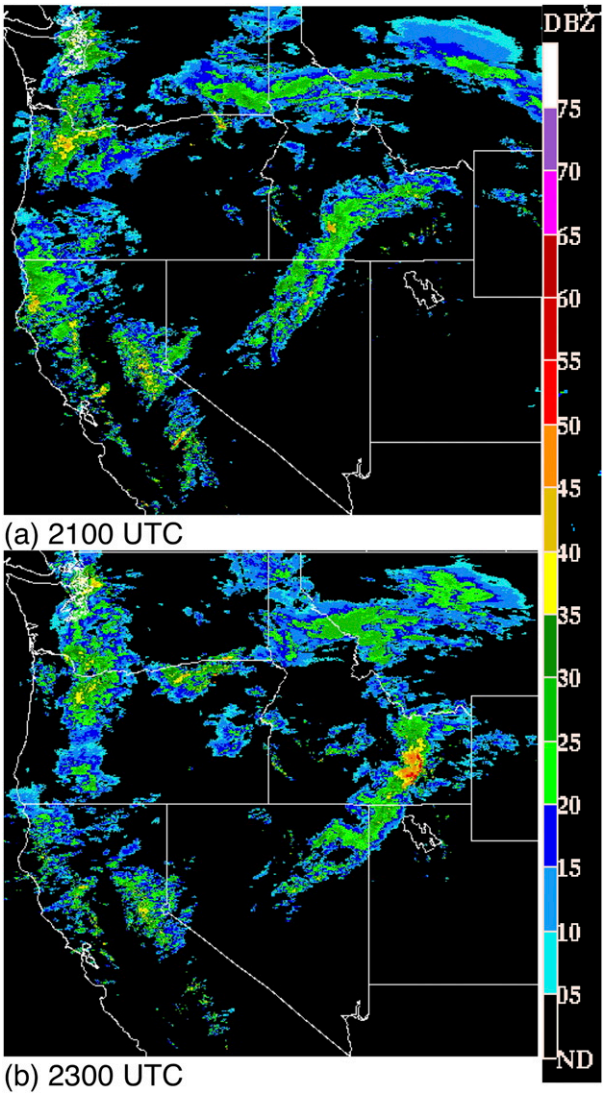

FIG. 5. Radar reflectivity factor (dBZ, according to scale) for 14 Feb 2000: (a) 2100 UTC and (b) 2300 UTC.

however, the bow echo had weakened, but the precipitation band remained strong as the convection moved into the mountains of southeast Idaho (Fig. 6c).

The precipitation band evolved from being well ahead of the lower-tropospheric cold advection at 1200 UTC 14 February to being at the leading edge of lower-tropospheric cold advection at 0000 UTC 15 February (cf. Figs. 3a–c and 6a–c). At 0000 UTC 15 February, the northern part of the band moved eastward into Wyoming and the southern part of the band stalled over northern Utah (Fig. 6c), eventually dissipating in central Utah by 1000 UTC 15 February (Schultz and Trapp 2003).

A crucial observation is that the components of the frontal system were moving rather quickly. The surface

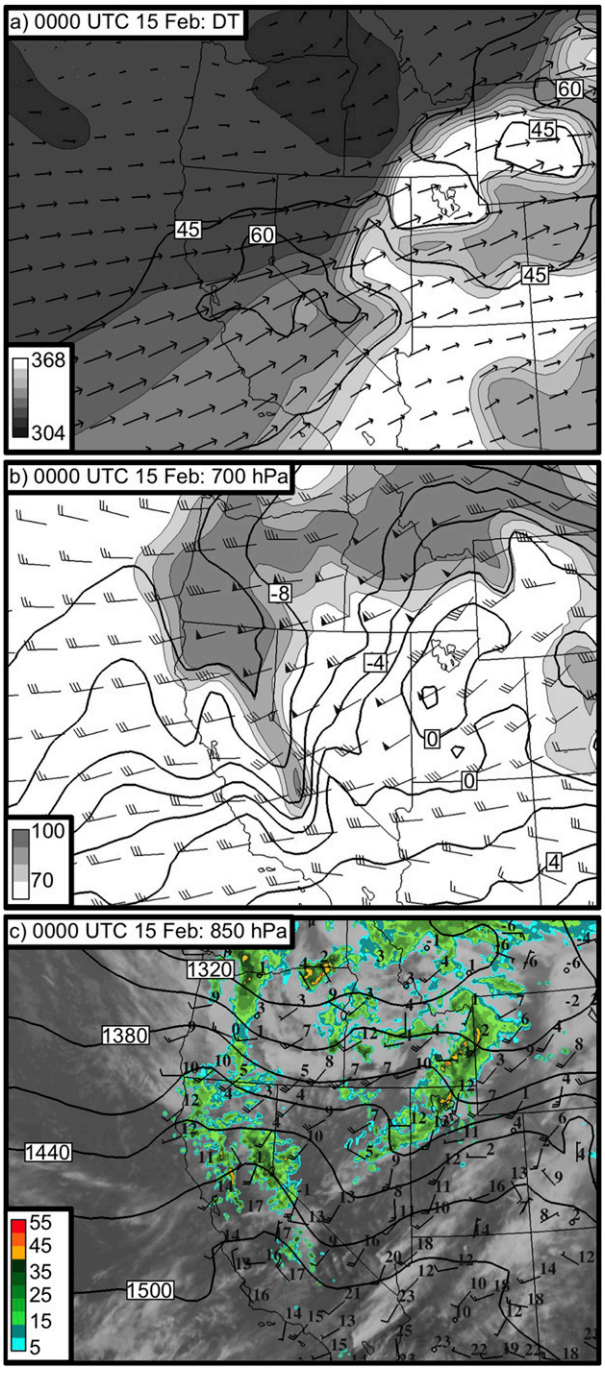

FIG. 6. Regional analyses from the RUC2 at 0000 UTC 15 Feb 2000. (a) Dynamic tropopause (DT) potential temperature (shaded every 8 K following inset scale), isotachs (contours at 45 and 60 m s^{-1}), and wind vectors. (b) 700-hPa temperatures (contours every 2°C), relative humidity greater than 70% (shaded every 10% following inset scale), and wind (pennants, full barbs, and half-barbs denote 25, 5, and 2.5 m s^{-1}, respectively). (c) 850-hPa geopotential height (contours every 30 m), NEXRAD 8-km composite radar reflectivity (greater than 5 dBZ color-filled following inset scale), infrared satellite imagery, and selected MesoWest surface observations of temperature (°C, upper right) and wind [barbs as in (b)].

pressure trough passed Oakland at 1200 UTC and reached Wendover, Utah, 780 km away, at 2300 UTC. These observations indicate an average speed of 19.6 m s^{-1}, which is faster than the component of the near-surface posttrough winds perpendicular to this trough of 5–15 m s^{-1} (as will be shown in the next sections). Explaining why this feature moved faster than the surface winds is key to understanding the forthcoming description of its evolution.

4. Landfall and passage across California

Time series from surface stations in and around northern California indicate the passage of two distinct features, labeled 1 and 2 in Fig. 7. The first feature passed through northern California around 1200–1400 UTC 14 February and was associated with the principal cloud band associated with the cyclone (Fig. 3c), although most of the precipitation had occurred prior to the arrival of this cloud band. This cloud band was associated with a minimum, then a strong increase, in altimeter setting with veering wind (Fig. 7). Winds over the lowest 3 km at profiler sites like the Sacramento Metropolitan Air Quality Management District's 915-MHz wind profiler at Sacramento show that this surface pressure trough was associated with the change from low-level veering to a unidirectional profile from the southwest (Fig. 8) and is consistent with the strengthening of the winds and the arrival of the upper-level trough onshore (Fig. 3a). The radar imagery and precipitation amounts showed an embedded line of convection with the heaviest precipitation occurring at this time (Fig. 3c). For example, Sacramento Executive Airport (SAC) received 21 mm (0.82 in.) of precipitation in 5 h with this feature (Fig. 7). The surface temperature with the passage of this feature, however, only dropped 1°–2°C at many stations, if at all (Fig. 7). The dewpoint temperature at the California stations rose or held steady until the passage of this feature, before falling after its passage (Fig. 7), likely associated with evaporating precipitation into the prefeature air mass before drier air following arrived. This vertical wind-shift line through the lowest 2 km is reminiscent of some of the features associated with landfalling frontal systems in Neiman et al. (2004, their Fig. 7) with the near-vertical boundary through the lowest 300 hPa (although their front was associated with the principal temperature drop of 2°C within about 20 min; their Fig. 8).

The second feature passed through northern California 4–6 h later. It passed the Monterey buoy 46042 between 1600 and 1700 UTC, identified primarily by veering of the wind (30° in one hour), but followed by a slow drop in temperature (1°C in 9 h) and a gentle rise in pressure (5.8 hPa in 6 h) (Fig. 7). Farther inland and after sunrise, however, the temperature drop became more sharply defined. At stations like Oakland (OAK), McClelland (MCC), Sacramento (SAC), and Stockton (SCK) (locations in Fig. 2), this feature passed around 1800–1900 UTC when the temperature dropped about 4°–6°C in an hour or two, and the rising pressure, which followed the first feature, began to level off (Fig. 7). The winds from the Sacramento wind profiler veered with time with the passage of the second feature from southwest to west-southwest at elevations less than about 1250 m (Fig. 8). This second feature was associated with a 200-km-long line of reflectivity that passed SAC at about 1800 UTC (Fig. 4c). A different southwest–northeast-oriented band associated with feature 2 moved to near Reno by 2100 UTC (Fig. 5a). This precipitation band had warmer cloud tops and produced less precipitation than the first band (Figs. 6c and 7). For example, SAC received only 0.25 mm (0.01 in.) with this band compared to 23.4 mm (0.92 in.) with the band associated with the surface pressure trough (Fig. 7).

Visible satellite imagery helps to distinguish these two features further (Fig. 9). At 1800 UTC, when the principal cloud band and its associated precipitation were reorganizing in the lee of the Sierra in western Nevada and southeastern Oregon (to be discussed further in section 5), the principal cloud band was continuous with a rope cloud over the Pacific Ocean (Fig. 9a). Despite the limited availability of visible imagery early in the morning, this rope cloud can be extrapolated back to northern California around 1200 UTC, when the first feature passed through northern California.

The second feature entered the San Francisco Bay Area at 1800 UTC (Fig. 9a). Clouds were loosely organizing over the ocean along the secondary feature (Fig. 9a), indicating some surface convergence, which can be inferred by the wind shift in station time series (Fig. 7). But, apparently, this feature did not organize sufficiently to develop into a rope cloud as the first feature did (Fig. 9b).

To summarize IPEX IOP 4 over northern California, its structure was characterized by two features. The first feature was associated with the principal cloud band associated with the cyclone and a surface pressure trough. Infrared satellite imagery indicated the clouds were deep, with heavy precipitation measured at the surface during the passage of this feature. Over the ocean, this feature was coincident with a rope cloud, which usually represents lower-tropospheric convergence and the leading edge of a surface front

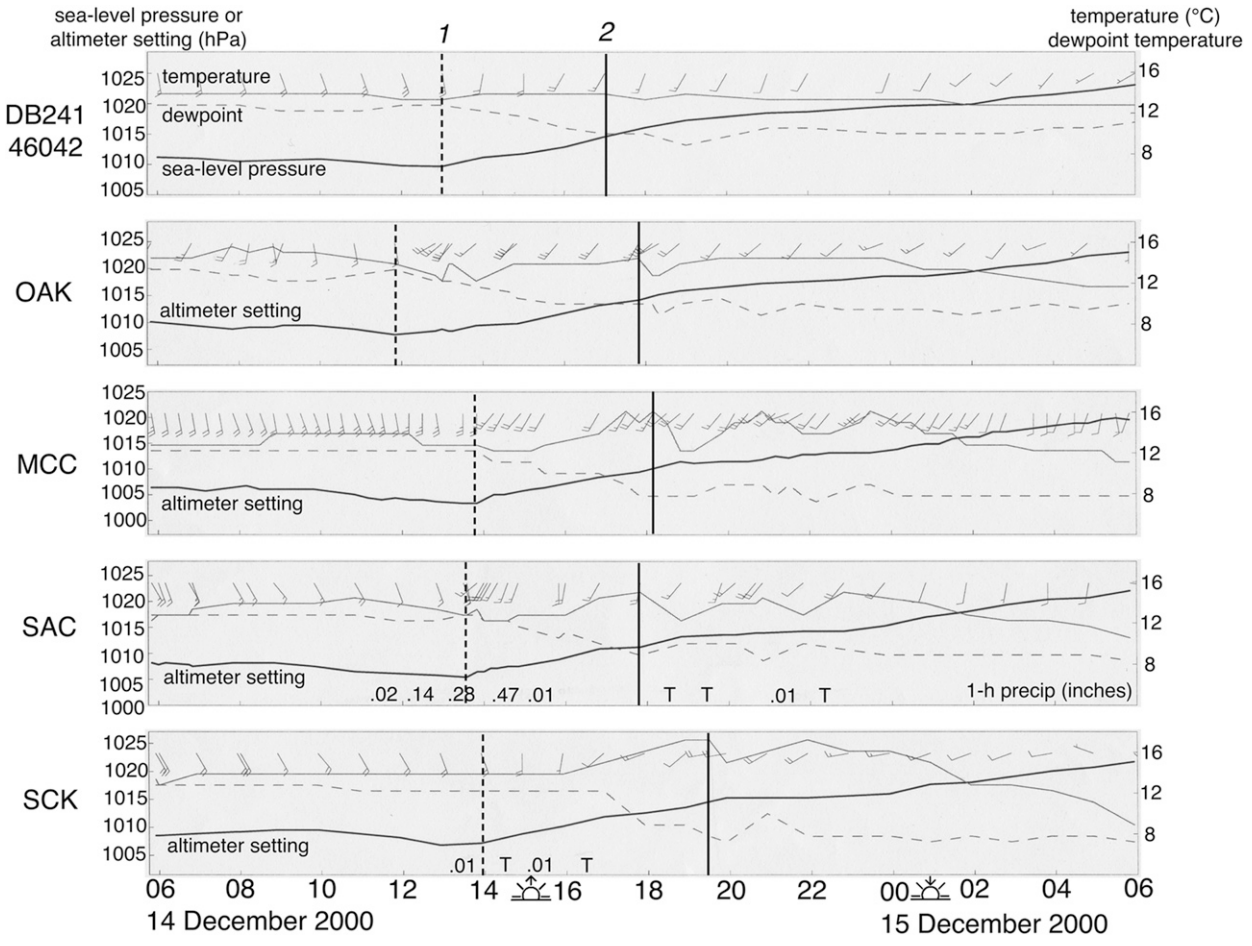

FIG. 7. Time series of weather from surface stations in California: buoy 50 km west-northwest of Monterey (46042), Oakland (OAK), McClelland (MCC), Sacramento (SAC), and Stockton (SCK). The dashed vertical lines labeled "1" represent the first feature (i.e., trough passage), and the solid lines labeled "2" represent the second feature. Notation for the wind is full barbs and half-barbs denote 5 and 2.5 m s^{-1}, respectively. Icons along time axis represent sunrise (sun with up arrow) and sunset (sun with down arrow).

(e.g., Shaughnessy and Wann 1973; Janes et al. 1976; Woods 1983; Seitter and Muench 1985; Shapiro et al. 1985; Shapiro and Keyser 1990, section 10.3.1). In this case, however, the surface temperature change and wind shift were generally small, so we choose not to call this feature a front, in agreement with Sanders and Doswell (1995) and Sanders (1999a), who argued for the primacy of temperature in frontal analysis. Instead, we refer to this first feature as the surface pressure trough, as that is its key defining characteristic.

The second feature, on the other hand, was associated with relatively modest satellite and radar signatures. Precipitation was light. The temperature fall associated with the passage of this feature, however, was larger than with the first feature. Because the structure of these features does not fit conveniently into the terminology of the Norwegian cyclone model (e.g., Bjerknes 1919; Bjerknes and Solberg 1921), we refer to both the two features together by the term *cold-frontal system*.

5. Passage across Nevada and to western Utah

Having documented the structure of this frontal system in California, we now examine its evolution as it moved into the lee of the Sierra Nevada. As Fig. 7 showed, stations west of the Sierra Nevada generally presented a consistent picture of the cyclone structure with two features comprising the frontal system. On the other side of the Sierra Nevada, however, the structure of the frontal system had changed.

The time series from Reno (RNO) looked qualitatively similar to those from California with the passage

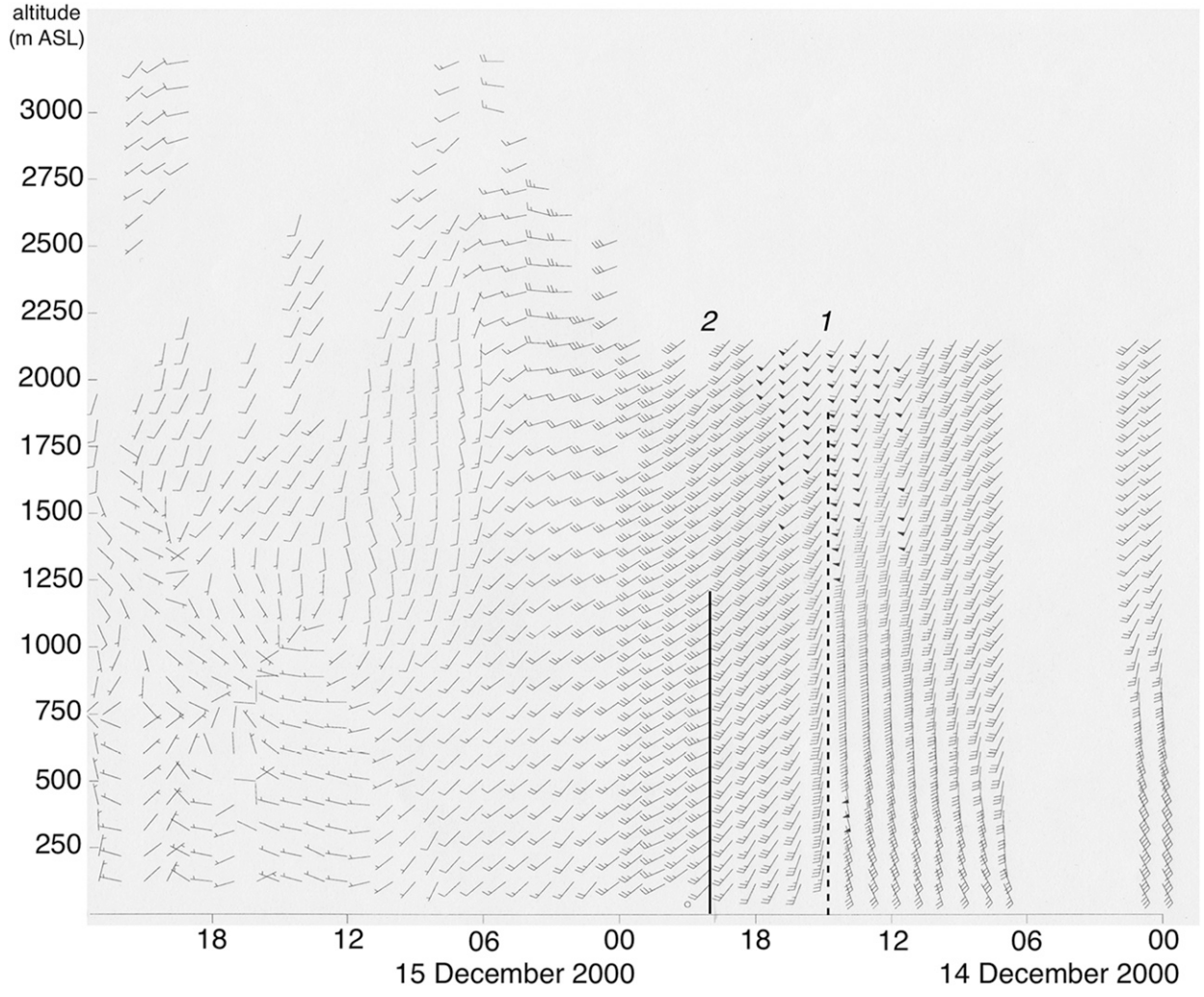

FIG. 8. Time–height series of wind from the Sacramento Metropolitan Air Quality Management District's 915-MHz wind profiler at Sacramento from 0000 UTC 14 Dec to 2300 UTC 15 Dec 2000. Notation for the wind is pennants, full barbs, and half-barbs denote 25, 5, and 2.5 m s^{-1}, respectively. The dashed vertical line labeled "1" represents the first feature (i.e., trough passage), and the solid line labeled "2" represents the second feature.

of the first feature (i.e., surface pressure trough) at 1500 UTC, followed by the passage of the second feature at 2000 UTC (cf. Figs. 7 and 10). As with the California stations, more precipitation fell at RNO with the surface pressure trough than with the second feature (6.6 mm versus 2.0 mm; 0.26 in. versus 0.08 in.). Within 135 km to the east, however, a dramatic change took place. Specifically, the largest temperature drop at Lovelock (LOL), Nevada, occurred at 1800–1900 UTC (7°C), consistent with the passage of the first feature (Fig. 10). The second feature weakened, becoming associated with a much slower rate of decrease in temperature (5°C over 3 h). Fallon Naval Air Station (not shown), only 100 km to the northeast of RNO, also showed similar features to that of LOL, indicating that this change in the structure of the front was not limited to just one station.

Thus, by the time the frontal system had moved past RNO, the surface pressure trough had developed the primary baroclinicity for the cold-frontal system shortly after sunrise. In addition, the temperature fall intensified substantially to about 8°C within an hour. After passing east of RNO, precipitation was only reported with the trough. For example, LOL and EKO received only 2.5 mm (0.1 in.) of precipitation each, precipitation that fell within an hour of the principal fall in temperature.

To understand the reasons for this change in structure of the cold-frontal system, we list the following pieces of evidence.

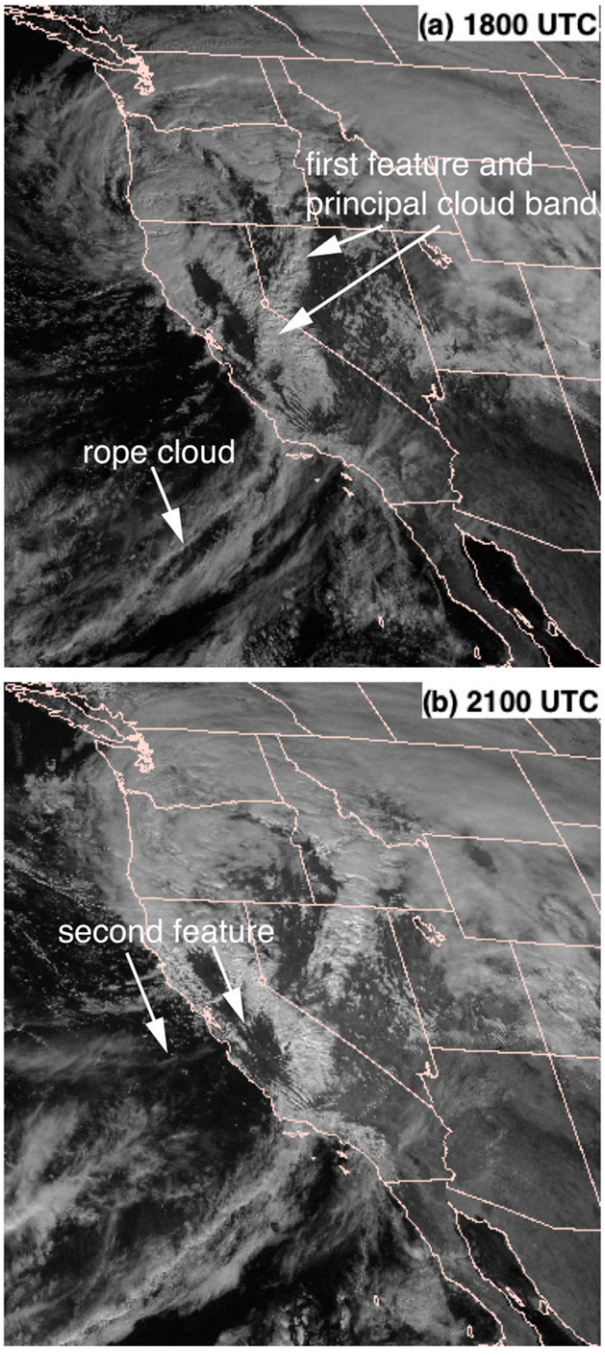

FIG. 9. *GOES-10* visible satellite imagery 14 Feb 2000: (a) 1800 UTC and (b) 2100 UTC.

1) The surface pressure trough appeared to pass across the Sierra Nevada relatively unimpeded (Figs. 7 and 10). A time series of stations in Nevada and western Utah shows the pressure minimum progressively moving from west to east, followed by a strong pressure rise (Fig. 10). This surface pressure trough was likely the 850-hPa trough in Fig. 4c and appeared to be related to forcing for surface pressure falls associated with the upper-level short-wave trough (Fig. 4a).
2) Downsloping winds may have cleared the skies, allowing for greater daytime heating from the sun, increasing the temperature ahead of the frontal system at some stations. The warming was likely enhanced by downslope warming in the lee of the Sierra Nevada, as discussed for a different case in West and Steenburgh (2011). Over Nevada and on a smaller scale, Wendover, Utah (ENV), on the Nevada–Utah border, experienced a 3°C warming and a 2°C decrease in dewpoint when the winds shifted out of the southwest at 2000 UTC and was downsloping off the adjacent Toano Mountain Range, perhaps also aided by mixing out of the overnight cold pool (Fig. 10).
3) Right before passage of the first feature, the temperatures rose, with the largest rises occurring at the easternmost stations in Nevada (Fig. 10). This temperature rise was partly due to daytime heating from the clear skies ahead of the cloud band across much of Nevada (Figs. 4c and 9a), which explains why the temperature rises occurred only after sunrise and were largest at the easternmost stations in Nevada, which had the longest time to be heated. Because the air ahead of the first feature was warmed, the temperature drop associated with the frontal system increased. These high temperatures were above normal for this time of year, which also indicated the warmth of the air in the ridge ahead of the trough. For example, the daily high temperature in EKO was about 12°C before passage of the first feature (Fig. 10), which is 6°C above its average high temperature for February.
4) The subsequent temperature drop associated with the first feature, however, only lasted a few hours. By 1900 UTC, temperatures in western Nevada had dropped by as much as 7.8°C with the winds from the southwest or west (Fig. 10). By 2000 UTC, temperatures in western Nevada had recovered about 2.8°C, which in another hour returned to nearly their original temperature before the passage of the first feature. The temperature recovery was associated with daytime heating. As the front moved farther eastward, passage occurred later in the day with less opportunity for heating. Hence, the temperature recovery was less.
5) The lower-tropospheric dewpoint depression (the difference between the air temperature and the dewpoint temperature) ahead of the first feature was much greater in Nevada (dewpoints about 3°C and dewpoint depressions as much as 12°C) than in California (dewpoints about 12°C in the Central Valley and dewpoint depressions about 5°C).

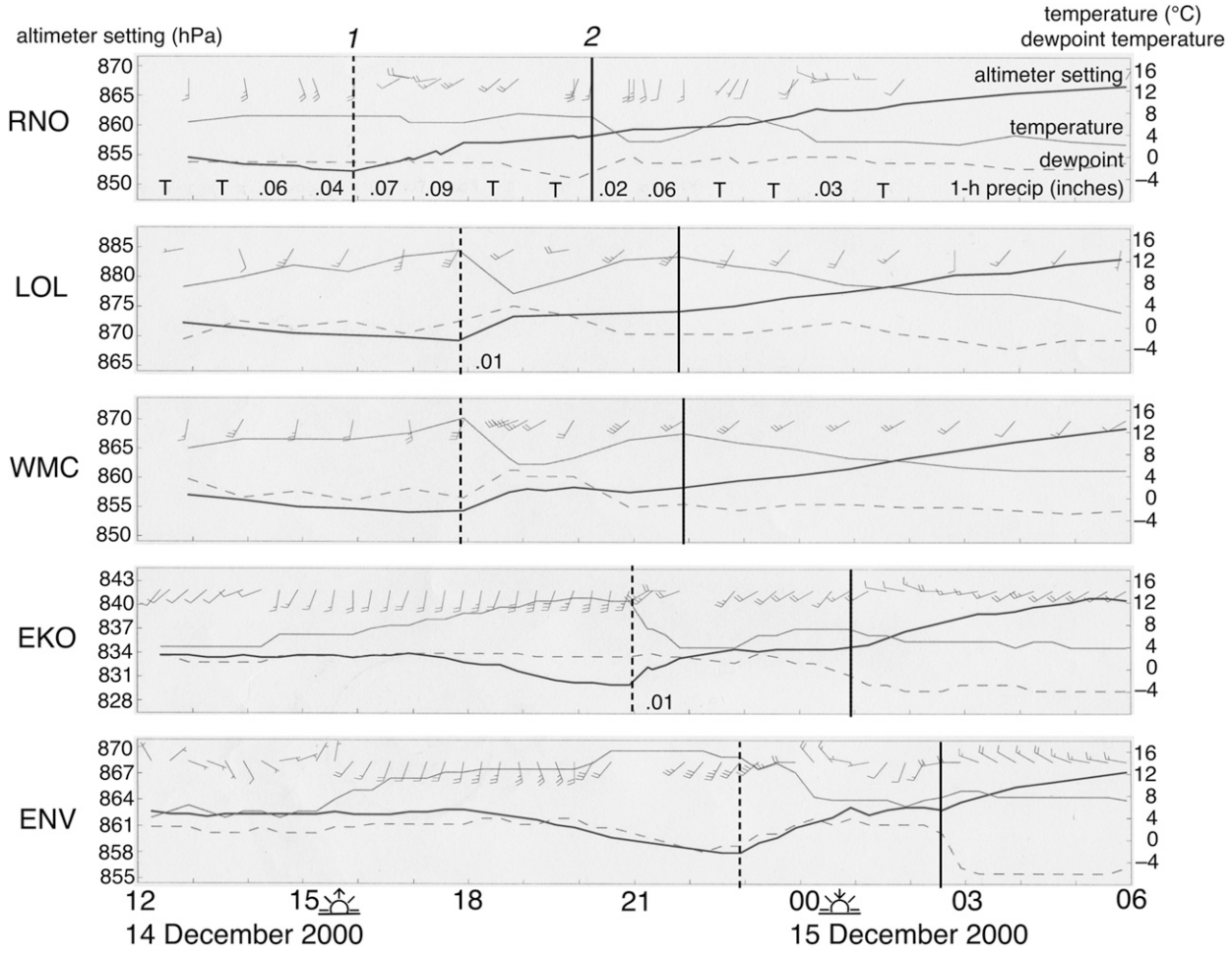

FIG. 10. Time series of weather from surface stations in Nevada and Utah: Reno (RNO), Lovelock (LOL), Winnemucca (WMC), Elko (EKO), and Wendover (ENV). The dashed vertical lines labeled "1" represent the first feature (i.e., trough passage), and the solid lines labeled "2" represent the second feature. Notation for the wind is full barbs and half-barbs denote 5 and 2.5 m s^{-1}, respectively. Icons along time axis represent sunrise (sun with up arrow) and sunset (sun with down arrow).

In other words, the lower troposphere was drier in Nevada and further from saturation.

6) After passing over the Sierra Nevada into Nevada, most of the precipitation associated with the frontal system was occurring at and west of the first feature (i.e., the trough). Thus, precipitation falling into the subsaturated subcloud air in Nevada led to evaporative cooling, which enhanced the temperature gradient, as indicated by cooling (and moistening) with the passage of the first feature at LOL, WMC, and ENV (Fig. 10).
7) The strong winds associated with the recorded gusts in Fig. 1 had unusual behaviors. Specifically, the wind gust at RNO occurred at 1730 UTC, after the pressure trough associated with the first feature, but before the temperature drop associated with the second feature. This situation was repeated at WMC with the gust occurring around 2100 UTC. However, the strongest gusts occurred before and at the time of the passage of the first feature at EKO and ENV.
8) After passage of the first feature, the pressure and dewpoint rose (Fig. 10), consistent with the creation of a mesohigh due to evaporation from precipitation aloft (e.g., Johnson 2001; Schultz and Trapp 2003). After the temperature rebounded, many stations in Nevada experienced a continued decline in temperature over time, in part due to cold advection (e.g., Figs. 4b and 6b) and in part due to being in the late afternoon and evening hours with reduced solar heating allowing net longwave cooling to dominate. At EKO and ENV, the wind shift associated with this second feature became much more dramatic, with postfeature westerlies and northwesterlies.
9) The second feature underwent a change from California and RNO when it was the dominant temperature drop

to central and eastern Nevada when the temperature gradient weakened (cf. Figs. 7 and 10). All of the central and eastern Nevada stations had a strong wind shift associated with this feature, but EKO and ENV stand out as being particularly strong (Fig. 10). It is unclear why the wind shift became more dramatic over time.

These observations depict the changes to the frontal system as it moved across the Sierra Nevada and across Nevada. The surface pressure trough advanced eastward in association with a short-wave trough aloft. Precipitation formed in association with this trough evaporated into the subcloud dry air, leading to cooling behind the first feature, contributing toward the main temperature gradient developing in conjunction with the first feature. Rising temperatures east of the first feature due to downslope warming and daytime heating further increased the temperature gradient across the first feature. Confluence in the lee of the Sierra Nevada also tightened the temperature gradient across the first feature. In this manner, the principal temperature drop associated with this cold-frontal system jumped from being associated with the second feature to the first feature, resembling a process of discrete frontal propagation (Charney and Fritsch 1999; Bryan and Fritsch 2000a,b; Steenburgh et al. 2009; West and Steenburgh 2010, 2011).

6. Synthesis

The characteristics of the cold-frontal system in IPEX IOP 4 bear similarities to previously documented fronts, and these characteristics have implications for conceptual models of cold fronts in the western United States, challenging the convention of a traditional cold front. This section summarizes this case by identifying its nonclassic characteristics in section 6a, comparing the frontal evolution of this case to that of other cases in section 6b, explaining the climatology of strong cold-frontal passages in section 6c, and concluding in section 6d.

a. IPEX IOP 4: A nonclassic cold-frontal system

Synthesizing these observations of the frontal system from offshore of California to its arrival in Utah, we suggest that its evolution occurred in ways that are inconsistent with traditional models of cold fronts.

1) A ROPE CLOUD DID NOT REPRESENT THE LOCATION OF THE STRONGEST TEMPERATURE DECREASE.

The first feature of the frontal system possessed a rope cloud over the ocean, ahead of the line with the larger temperature drop and more modest radar and satellite signatures. Conventional wisdom is that a rope cloud represents the location of the surface cold front (e.g., Shaughnessy and Wann 1973; Janes et al. 1976; Woods 1983; Seitter and Muench 1985; Shapiro et al. 1985; Shapiro and Keyser 1990, section 10.3.1). Thus, having a rope cloud along a trough without a strong temperature gradient challenges our notion of what these features may represent in some cases. Although rope clouds may be associated with strong convergence, they may not be associated with the strongest baroclinicity, as shown in this present case.

2) THE LANDFALLING COLD-FRONTAL SYSTEM COMPRISED MULTIPLE FEATURES.

This frontal system at landfall was associated with a surface pressure trough ahead of the second feature that had the larger temperature decrease (although still weak in an absolute sense). This kind of complexity of multiple features associated with frontal systems has been observed in other cases of landfalling Pacific frontal systems (e.g., Neiman et al. 2004) and beyond. For example, Schultz (2005) documented ten different types of prefrontal troughs and wind shifts associated with cold fronts. In other examples, multiple cold and warm fronts within extratropical cyclones have been documented over the North Atlantic Ocean on the Met Office surface charts (Mulqueen and Schultz 2015) and over the eastern United States (Metz et al. 2004). All of these examples of cyclones with multiple features comprising frontal systems differ from the classic conceptual model of cyclones and fronts.

3) TEMPERATURE DECREASES ASSOCIATED WITH THE FEATURES IN CALIFORNIA WERE RELATIVELY WEAK.

Although the temperature decreases associated with fronts over the ocean are reduced because of the moderating influence of the underlying ocean surface, once onshore, the temperature gradient associated with the first feature in IPEX IOP 4 increased, but still remained relatively weak. In fact, the pressure trough was the most prominent characteristic of this frontal system, a point noted by other authors for other cases. For example, Williams (1969, p. 27) wrote about frontal passages at Sacramento: ''Temperature contrasts are weak across frontal zones, and pressure tendencies are the most reliable indicators of frontal passages.'' McClain and Danielsen (1955) described cases with weak baroclinicity below 700 hPa and estimated that one-third of all landfalling Pacific troughs were nonfrontal.

4) THE SURFACE PRESSURE TROUGH REPRESENTED THE SHORT-WAVE TROUGH ALOFT.

This mobile surface pressure trough was associated with the steady eastward motion of an upper-level

trough across the western United States that brought an end to the warm advection aloft and indicated the onset of cold advection. Such surface pressure troughs can help locate upper-level short-wave troughs that might otherwise be disrupted by local effects in regions of complex topography (e.g., Hess and Wagner 1948; Schultz and Doswell 2000).

5) THE COLD-FRONTAL SYSTEM MOVED FASTER THAN THE POSTSYSTEM WIND SPEED.

From landfall in California to arrival at Utah, the pressure trough associated with the frontal system traveled at about 20 m s^{-1}, a speed higher than most of the postfrontal winds normal to the front at the surface and in the lower troposphere. Here, the postfrontal surface winds can be inferred from those plotted in Figs. 7 and 10. In California, surface winds within an hour or two of passage of the first feature are out of the southwest at 25 kts (13 m s^{-1}) (Fig. 7), but the orientation of the front is southwest–northeast. Thus, surface postfrontal winds are almost parallel to the front. In Nevada, surface postfrontal winds are 20–30 kts (10–15 m s^{-1}), and even when nearly perpendicular to the front (as in EKO in Fig. 10) would not account for the motion of the front.

Even considering the winds above the surface, the postfrontal winds aloft behind the first feature in the Sacramento wind profiler (Fig. 8) are more than 40 kts (20 m s^{-1}) at about 1300 m—and even then still nearly parallel to the front. At 700 hPa, the postfrontal wind speed can be 60–75 kt (30–38 m s^{-1}) in Figs. 4b and 6b, but that is at an angle of 30° to the temperature gradient [sin(30°) = 0.5], so half of 30–38 m s^{-1} would barely bring it to the 20 m s^{-1} speed of the front in the best possible situation. Thus, it is hard to imagine that the winds aloft explain the movement of the front either.

For the front to move faster than the postfrontal winds, the generation of the evaporatively cooled air needed to replenish the immediate postsystem air. Both the case described by Steenburgh et al. (2009) and the present case have the surface front moving at the same speed as the shortwave trough aloft. The propagation of fronts (i.e., motion faster than by advection) in the western United States has been observed previously, as well. Williams (1972, p. 1) wrote "the analysis of cold fronts themselves is subject to limitations," including "the failure to move cold fronts along with the surface gradient, or, more precisely, with the speed of low-level winds in the cold air-mass normal to the front." Specifically, a "check on frontal positions can be made by association with short-wave troughs as shown on upper-air charts, preferably at the 500-mb level. Cold fronts in [the] western United States usually lie in the area of positive vorticity advection ahead of a short-wave trough" (p. 2).

6) DISCRETE FRONTAL PROPAGATION OCCURRED IN THE LEE OF THE SIERRA NEVADA.

Although the surface pressure trough (i.e., the first feature) was associated with a band of precipitation in California, its temperature drop was small. Only when precipitation fell into the drier subcloud air in the lee of the Sierra Nevada did evaporation lead to stronger cooling and less precipitation reaching the surface. In combination with confluence in the lee of the Sierra Nevada, downslope warming, and solar heating ahead of the trough, the temperature gradient across the trough intensified, eventually becoming the dominant baroclinic zone in the frontal system. That the cooling (and moistening) lasted for only a few hours is consistent with a locally generated source of cold air, rather than postfrontal advection of a synoptic-scale maritime polar air mass (e.g., Schultz and Trapp 2003). This evolution of the frontal system is reminiscent of the discrete frontal propagation described by Charney and Fritsch (1999) and Bryan and Fritsch (2000a,b), but applied to frontal movement across the Sierra Nevada by Steenburgh et al. (2009) and West and Steenburgh (2010, 2011).

7) SUBCLOUD EVAPORATION WAS ALREADY ALTERING THE FRONTAL STRUCTURE IN NEVADA.

As the front moved into northern Utah, Schultz and Trapp (2003) described its structure due to subcloud evaporation and sublimation of precipitation. The subcloud dry air and evaporation of subcloud precipitation was in part responsible for the formation of mammatus on the underside of the clouds associated with the front (Schultz et al. 2006, 2418–2420), indicating a cloudy layer atop a dry subcloud layer (Kanak et al. 2008). What our analysis of this event shows is that the alteration of the frontal structure by diabatic cooling had already been underway for 6 h, starting shortly after crossing the Sierra Nevada.

b. Comparison to other cases

In IPEX IOP 4, a number of processes led to the intensification of the temperature gradient across the first feature (i.e., the surface pressure trough). For example, warming downslope flow cleared clouds and allowed sensible daytime heating ahead of the surface pressure trough. Behind the trough, subcloud evaporation or sublimation cooled the lower troposphere, further enhancing the temperature difference. Such temperature differences across fronts can lead to cross-frontal circulations that intensify them further

(e.g., Koch et al. 1995), at least for a short time (e.g., Sanders 1999b).

Once created, such temperature differences across fronts can be intensified by confluence of air masses in the lee of the Sierra Nevada. The magnitude of this confluence is likely related to the upper-level forcing as it moves through the Intermountain West. When a number of different cases of cyclone evolution through the West are examined, a key difference between these cases is the latitude, intensity, and orientation of the upper-level trough, affecting the magnitude of the confuence in the lee of the Sierra Nevada.

1) Sanders (1999b) studied an upper-level short-wave trough associated with a surface front across the southwest United States that lasted for about 18 h and was associated with the strongest temperature gradient during diurnal heating. The importance of the diabatic heating ahead of the front is similar to the intensification of the frontal system in Nevada during IPEX IOP 4. However, no substantial cooling due to evaporating precipitation occurred behind the front in Sanders's case (e.g., Sanders 1999b, his Fig. 5b and p. 2402).
2) West and Steenburgh (2010) examined a persistent case of confluence downstream of the Sierra Nevada that also featured intense Intermountain cyclogenesis during the Tax Day Storm. The shortwave trough was compact and intense, with the strongest forcing for pressure falls (related to the highest pressures on the dynamic tropopause) south of Lake Tahoe. The resulting 850-hPa low pressure center was well defined with strong troughing and cyclogenesis (West and Steenburgh 2010, their Fig. 9a). The confluence served as the locus for the frontogenesis (i.e., the "collector of fronts" as described by Petterssen 1940, p. 255, and discussed by Cohen and Schultz 2005, p. 1359), but differential diabatic processes were also important for frontal development. In West and Steenburgh (2010), confluence, sensible heating, and postfrontal subcloud cooling were all important to the resulting strengthening of the temperature gradient across the front.
3) Steenburgh et al. (2009) and West and Steenburgh (2011) examined another case (25 March 2006) which featured a transient frontal system and discrete propagation. In this case, the trough was more mobile and more negatively tilted, with the strongest forcing for surface pressure falls north of Lake Tahoe. In this case, confluence was essential for the development and discrete propagation of the front, with differential diabatic heating contributing to the intensity of the front.
4) The strongest forcing in IPEX IOP4 tracks even farther north (over Oregon) compared to these previous cases, and no surface cyclone is present over the West (Fig. 6c). Without a surface cyclone, lee-side confluence is weaker and contributes less to the development and intensification of the front than in the cases described by Steenburgh et al. (2009) and West and Steenburgh (2010, 2011). In IPEX IOP 4, downslope warming, sensible heating, and postfrontal subcloud cooling appeared to be most important, with confluence of secondary importance.

Synthesizing this case with others in the literature confirms the variety of ways that the temperature gradient and the forcing for surface pressure falls can lead to different structures and evolutions. Thus, the variety in the structure and evolution of these cases is determined by the relative importance of these various processes to frontal structure and evolution in the Intermountain West.

c. *Explaining the climatology of strong cold-frontal passages*

This present case—as well as previously published cases—is consistent with the climatology of strong cold-frontal passages in the western United States by Shafer and Steenburgh (2008). They defined a strong cold-frontal passage as "1) a surface temperature fall of at least 7°C over a 2–3-h period, 2) a corresponding altimeter pressure rise of at least 3 hPa, and 3) the presence of a 700-hPa temperature gradient of at least 6°C $(500\,\text{km})^{-1}$" (Shafer and Steenburgh 2008, p. 786). They found a large gradient in the frequency of strong cold-frontal passages across the western United States (Fig. 11). Strong cold-frontal passages are at a minimum along the Pacific coast where the influence of mild ocean air limits the formation of strong cold fronts (0–3 events over the 25-yr period 1979–2003). In contrast, a maximum in frontal passages lies immediately east of the Front Range of the Rockies (150–300 events over 25 years), where strong cold fronts typically arise from cold air associated with the equatorward movement of polar anticyclones meeting warmer air from the Gulf of Mexico (e.g., Dallavalle and Bosart 1975; Rogers and Rohli 1991; Mecikalski and Tilley 1992; Schultz et al. 1997, 1998). The Rockies generally block the movement of such shallow Arctic air from making it to the Intermountain West, limiting strong cold-frontal passages from this direction.

The Intermountain West can also be visited by strong cold fronts (10–100 events over 25 years), with the number of frontal passages increasing from west to east across central Nevada and eastern Oregon, reaching the

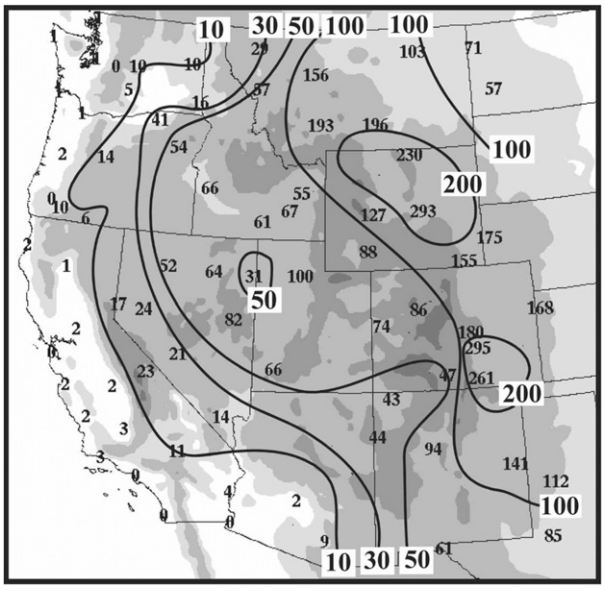

FIG. 11. Total number of strong cold-frontal passages (1979–2003) with contours of 10, 30, 50, 100, and 200 events. Terrain shaded at intervals of 0.5, 1, 2, and 3 km. Figure and caption adapted from Shafer and Steenburgh (2008, their Fig. 4).

local maximum at Salt Lake City in northern Utah (Fig. 11). This increase in frontal passages happens due to both diabatic processes (e.g., surface diurnal heating in the warm air, evaporation of precipitation in the cold air) and strengthening of the front associated with confluence in the lee of the Sierra. Both of these processes would favor an increasing frequency of strong frontal passages away from the lee of the Sierra.

d. Conclusions

The observations of the cold-frontal system in this article challenge the conceptual models of cold fronts. As with other cases in the literature, the frontal system in IPEX IOP 4 was not a classic cold front as would be found in a textbook. The frontal system was composed of two features. A rope cloud was associated with a convergence line, not the principal region of baroclinicity. The surface pressure trough, tied to the short-wave trough aloft, moved faster than the winds behind it, resulting in a form of discrete frontal propagation due to the replenishment of the cold air from aloft due to evaporative cooling ahead of the frontal system. The discrete propagation of the front also addresses the question that the near-surface postfrontal air that makes landfall on the California coast is not the same postfrontal air in Nevada and Utah. That air would have to be diabatically modified in situ from air with dramatically different origins. If the postfrontal air mass is not responsible for the motion of the cold front, then the conventional explanation for how cold fronts move in regions of complex terrain becomes a relevant question for synoptic meteorology. Thus, we present another case in which the diabatic processes (both evaporative cooling and sensible heating) and the confluence in the lee of the Sierra Nevada contribute to frontal intensification and discrete propagation.

Acknowledgments. We have benefited considerably from discussions with and comments from Jason Shafer, John Horel, Greg West, and Colby Neuman, and Larry Dunn. We appreciate the comments from two anonymous reviewers that have improved this manuscript. Additional assistance and input was provided by Justin Cox and Mark Jackson. The Storm Prediction Center graciously provided access to their archives of surface and upper-air maps and data. David White provided the NOAA/ETL profiler data. Special thanks go to John Horel, Mike Splitt, Judy Pechmann, and MesoWest (Horel et al. 2002) for providing radar and surface data. Thanks also to the governmental agencies, commercial firms, and educational institutions that provide data to MesoWest and make this type of research possible. Funding for the field phase of IPEX was provided by the NOAA National Severe Storms Laboratory Director's Discretionary Fund, NOAA Cooperative Institute for Regional Prediction at the University of Utah Grants NA87WA0351 and NA97WA0227, and the Utah Department of Transportation. Much of the research on this case was performed during fall 2002 while Schultz was visiting the then Department of Meteorology at the University of Utah; their support is gratefully acknowledged. Partial funding for Schultz was provided by NOAA/OAR/NSSL under NOAA–OU Cooperative Agreement NA17RJ1227 (1998–2006) and by the U.K. Natural Environment Research Council through Grants NE/I005234/1, NE/I024984/1, and NE/N003918/1 (2010–19). Partial funding for Steenburgh was provided by National Science Foundation Grants ATM-0627937 and ATM-0085318 and a series of grants from the NOAA/National Weather Service CSTAR Program. The opinions, findings, recommendations, and conclusions expressed in this article are those of the authors and do not reflect the official policy or position of the University of Utah, National Science Foundation, or NOAA/National Weather Service.

REFERENCES

Benjamin, S. G., J. M. Brown, K. J. Brundage, B. E. Schwartz, T. G. Smirnova, and T. L. Smith, 1998: The operational RUC-2. Preprints, *16th Conf. on Weather Analysis and Forecasting,* Phoenix, AZ, Amer. Meteor. Soc., 249–252.

Bjerknes, J., 1919: On the structure of moving cyclones. *Geofys. Publ.*, **1** (2), 1–8.

——, and H. Solberg, 1921: Meteorological conditions for the formation of rain. *Geofys. Publ.*, **2** (3), 1–60.

Bluestein, H. B., 1993: *Synoptic–Dynamic Meteorology in Midlatitudes. Volume II: Observations and Theory of Weather Systems*. Oxford University Press, 594 pp.

Bryan, G. H., and J. M. Fritsch, 2000a: Discrete propagation of surface fronts in a convective environment: Observations and theory. *J. Atmos. Sci.*, **57**, 2041–2060, https://doi.org/10.1175/1520-0469(2000)057<2041:DPOSFI>2.0.CO;2.

——, and ——, 2000b: Diabatically driven discrete propagation of surface fronts: A numerical analysis. *J. Atmos. Sci.*, **57**, 2061–2079, https://doi.org/10.1175/1520-0469(2000)057<2061:DDDPOS>2.0.CO;2.

Burke, P. C., and D. M. Schultz, 2004: A 4-yr climatology of cold-season bow echoes over the continental United States. *Wea. Forecasting*, **19**, 1061–1074, https://doi.org/10.1175/811.1.

Charney, J. J., and J. M. Fritsch, 1999: Discrete frontal propagation in a nonconvective environment. *Mon. Wea. Rev.*, **127**, 2083–2101, https://doi.org/10.1175/1520-0493(1999)127<2083:DFPIAN>2.0.CO;2.

Cohen, R. A., and D. M. Schultz, 2005: Contraction rate and its relationship to frontogenesis, the Lyapunov exponent, fluid trapping, and airstream boundaries. *Mon. Wea. Rev.*, **133**, 1353–1369, https://doi.org/10.1175/MWR2922.1.

Colle, B. A., J. B. Wolfe, W. J. Steenburgh, D. E. Kingsmill, J. A. Cox, and J. C. Shafer, 2005: High-resolution simulations and microphysical validation of an orographic precipitation event over the Wasatch Mountains during IPEX IOP3. *Mon. Wea. Rev.*, **133**, 2947–2971, https://doi.org/10.1175/MWR3017.1.

Cox, J. A., W. J. Steenburgh, D. E. Kingsmill, J. C. Shafer, B. A. Colle, O. Bousquet, B. F. Smull, and H. Cai, 2005: The kinematic structure of a Wasatch Mountain winter storm during IPEX IOP3. *Mon. Wea. Rev.*, **133**, 521–542, https://doi.org/10.1175/MWR-2875.1.

Dallavalle, J. P., and L. F. Bosart, 1975: A synoptic investigation of anticyclogenesis accompanying North American polar air outbreaks. *Mon. Wea. Rev.*, **103**, 941–957, https://doi.org/10.1175/1520-0493(1975)103<0941:ASIOAA>2.0.CO;2.

Hess, S. L., and H. Wagner, 1948: Atmospheric waves in the northwestern United States. *J. Meteor.*, **5**, 1–19, https://doi.org/10.1175/1520-0469(1948)005<0001:AWIENU>2.0.CO;2.

Horel, J., and Coauthors, 2002: MesoWest: Cooperative mesonets in the western United States. *Bull. Amer. Meteor. Soc.*, **83**, 211–225, https://doi.org/10.1175/1520-0477(2002)083<0211:MCMITW>2.3.CO;2.

Janes, S. A., H. W. Brandli, and J. W. Orndorff, 1976: "The blue line" depicted on satellite imagery. *Mon. Wea. Rev.*, **104**, 1178–1181, https://doi.org/10.1175/1520-0493(1976)104<1178:BLDOSI>2.0.CO;2.

Johnson, R. H., 2001: Surface mesohighs and mesolows. *Bull. Amer. Meteor. Soc.*, **82**, 13–31, https://doi.org/10.1175/1520-0477(2001)082<0013:SMAM>2.3.CO;2.

Kanak, K. M., J. M. Straka, and D. M. Schultz, 2008: Numerical simulation of mammatus. *J. Atmos. Sci.*, **65**, 1606–1621, https://doi.org/10.1175/2007JAS2469.1.

Koch, S. E., J. T. McQueen, and V. M. Karyampudi, 1995: A numerical study of the effects of differential cloud cover on cold frontal structure and dynamics. *J. Atmos. Sci.*, **52**, 937–964, https://doi.org/10.1175/1520-0469(1995)052<0937:ANSOTE>2.0.CO;2.

LaDue, J. G., 2002: The structure of a tornadic bow echo in Idaho. Preprints, *21st Conf. on Severe Local Storms,* San Antonio, TX, Amer. Meteor. Soc., 490–493.

McClain, E. P., and E. F. Danielsen, 1955: Zonal distribution of baroclinity for three Pacific storms. *J. Meteor.*, **12**, 314–323, https://doi.org/10.1175/1520-0469(1955)012<0314:ZDOBFT>2.0.CO;2.

Mecikalski, J. R., and J. S. Tilley, 1992: Cold surges along the Front Range of the Rocky Mountains: Development of a classification scheme. *Meteor. Atmos. Phys.*, **48**, 249–271, https://doi.org/10.1007/BF01029572.

Metz, N. D., D. M. Schultz, and R. H. Johns, 2004: Extratropical cyclones with multiple warm-front-like baroclinic zones and their relationship to severe convective storms. *Wea. Forecasting*, **19**, 907–916, https://doi.org/10.1175/1520-0434(2004)019<0907:ECWMWB>2.0.CO;2.

Mulqueen, K. C., and D. M. Schultz, 2015: Non-classic extratropical cyclones on Met Office sea-level pressure charts: Double cold and warm fronts. *Weather*, **70**, 100–105, https://doi.org/10.1002/wea.2463.

Neiman, P. J., F. M. Ralph, P. O. Persson, A. B. White, D. P. Jorgensen, and D. E. Kingsmill, 2004: Modification of fronts and precipitation by coastal blocking during an intense landfalling winter storm in southern California: Observations during CALJET. *Mon. Wea. Rev.*, **132**, 242–273, https://doi.org/10.1175/1520-0493(2004)132<0242:MOFAPB>2.0.CO;2.

NOAA, 2000: *Storm Data*. Vol. 42, No. 2, 127 pp.

Petterssen, S., 1936: Contribution to the theory of frontogenesis. *Geofys. Publ.*, **11** (6), 1–27.

——, 1940: *Weather Analysis and Forecasting*, McGraw-Hill, 505 pp.

Ralph, F. M., P. J. Neiman, and G. A. Wick, 2004: Satellite and CALJET aircraft observations of atmospheric rivers over the eastern North Pacific Ocean during the winter of 1997/98. *Mon. Wea. Rev.*, **132**, 1721–1745, https://doi.org/10.1175/1520-0493(2004)132<1721:SACAOO>2.0.CO;2.

Reynolds, D. W., and A. P. Kuciauskas, 1988: Remote and in situ observations of Sierra Nevada winter mountain clouds: Relationships between mesoscale structure, precipitation, and liquid water. *J. Appl. Meteor.*, **27**, 140–156, https://doi.org/10.1175/1520-0450(1988)027<0140:RAISOO>2.0.CO;2.

Rogers, J. C., and R. V. Rohli, 1991: Florida citrus freezes and polar anticyclones in the Great Plains. *J. Climate*, **4**, 1103–1113, https://doi.org/10.1175/1520-0442(1991)004<1103:FCFAPA>2.0.CO;2.

Rust, W. D., and R. J. Trapp, 2002: Initial balloon soundings of the electric field in winter nimbostratus clouds in the USA. *Geophys. Res. Lett.*, **29**, 1959, https://doi.org/10.1029/2002GL015278.

Rutz, J. J., W. J. Steenburgh, and F. M. Ralph, 2014: Climatological characteristics of atmospheric rivers and their inland penetration over the western United States. *Mon. Wea. Rev.*, **142**, 905–921, https://doi.org/10.1175/MWR-D-13-00168.1.

Sanders, F., 1955: An investigation of the structure and dynamics of an intense surface frontal zone. *J. Meteor.*, **12**, 542–552, https://doi.org/10.1175/1520-0469(1955)012<0542:AIOTSA>2.0.CO;2.

——, 1999a: A proposed method of surface map analysis. *Mon. Wea. Rev.*, **127**, 945–955, https://doi.org/10.1175/1520-0493(1999)127<0945:APMOSM>2.0.CO;2.

——, 1999b: A short-lived cold front in the southwestern United States. *Mon. Wea. Rev.*, **127**, 2395–2403, https://doi.org/10.1175/1520-0493(1999)127<2395:ASLCFI>2.0.CO;2.

——, and C. A. Doswell III, 1995: A case for detailed surface analysis. *Bull. Amer. Meteor. Soc.*, **76**, 505–521, https://doi.org/10.1175/1520-0477(1995)076<0505:ACFDSA>2.0.CO;2.

Saucier, W. J., 1955: *Principles of Meteorological Analysis*. University of Chicago Press, 438 pp.

Schultz, D. M., 2005: A review of cold fronts with prefrontal troughs and wind shifts. *Mon. Wea. Rev.*, **133**, 2449–2472, https://doi.org/10.1175/MWR2987.1.

——, and C. A. Doswell III, 2000: Analyzing and forecasting Rocky Mountain lee cyclogenesis often associated with strong winds. *Wea. Forecasting*, **15**, 152–173, https://doi.org/10.1175/1520-0434(2000)015<0152:AAFRML>2.0.CO;2.

——, and R. J. Trapp, 2003: Nonclassical cold-frontal structure caused by dry subcloud air in northern Utah during the Intermountain Precipitation Experiment (IPEX). *Mon. Wea. Rev.*, **131**, 2222–2246, https://doi.org/10.1175/1520-0493(2003)131<2222:NCSCBD>2.0.CO;2.

——, W. E. Bracken, L. F. Bosart, G. J. Hakim, M. A. Bedrick, M. J. Dickinson, and K. R. Tyle, 1997: The 1993 Superstorm cold surge: Frontal structure, gap flow, and tropical impact. *Mon. Wea. Rev.*, **125**, 5–39; Corrigendum, **125**, 662, https://doi.org/10.1175/1520-0493(1997)125<0005:TSCSFS>2.0.CO;2.

——, ——, and ——, 1998: Planetary- and synoptic-scale signatures associated with Central American cold surges. *Mon. Wea. Rev.*, **126**, 5–27, https://doi.org/10.1175/1520-0493(1998)126<0005:PASSSA>2.0.CO;2.

——, and Coauthors, 2002: Understanding Utah winter storms: The Intermountain Precipitation Experiment. *Bull. Amer. Meteor. Soc.*, **83**, 189–210, https://doi.org/10.1175/1520-0477(2002)083<0189:UUWSTI>2.3.CO;2.

——, and Coauthors, 2006: The mysteries of mammatus clouds: Observations and formation mechanisms. *J. Atmos. Sci.*, **63**, 2409–2435, https://doi.org/10.1175/JAS3758.1.

Seitter, K. L., and H. S. Muench, 1985: Observation of a cold front with rope cloud. *Mon. Wea. Rev.*, **113**, 840–848, https://doi.org/10.1175/1520-0493(1985)113<0840:OOACFW>2.0.CO;2.

Shafer, J. C., and W. J. Steenburgh, 2008: Climatology of strong Intermountain cold fronts. *Mon. Wea. Rev.*, **136**, 784–807, https://doi.org/10.1175/2007MWR2136.1.

——, ——, J. A. Cox, and J. P. Monteverdi, 2006: Terrain influences on synoptic storm structure and mesoscale precipitation distribution during IPEX IOP3. *Mon. Wea. Rev.*, **134**, 478–497, https://doi.org/10.1175/MWR3051.1.

Shapiro, M. A., and D. Keyser, 1990: Fronts, jet streams and the tropopause. *Extratropical Cyclones, The Erik Palmén Memorial Volume*, C. W. Newton and E. O. Holopainen, Eds., Amer. Meteor. Soc., 167–191.

——, T. Hampel, D. Rotzoll, and F. Mosher, 1985: The frontal hydraulic head: A micro-α scale (~1 km) triggering mechanism for mesoconvective weather systems. *Mon. Wea. Rev.*, **113**, 1166–1183, https://doi.org/10.1175/1520-0493(1985)113<1166:TFHHAM>2.0.CO;2.

Shaughnessy, J. E., and T. C. Wann, 1973: Frontal rope in the North Pacific. *Mon. Wea. Rev.*, **101**, 774–776, https://doi.org/10.1175/1520-0493(1973)101<0774:POTM>2.3.CO;2.

Smith, R. K., and M. J. Reeder, 1988: On the movement and low-level structure of cold fronts. *Mon. Wea. Rev.*, **116**, 1927–1944, https://doi.org/10.1175/1520-0493(1988)116<1927:OTMALL>2.0.CO;2.

Steenburgh, W. J., and T. R. Blazek, 2001: Topographic distortion of a cold front over the Snake River Plain and central Idaho mountains. *Wea. Forecasting*, **16**, 301–314, https://doi.org/10.1175/1520-0434(2001)016<0301:TDOACF>2.0.CO;2.

——, C. R. Neuman, G. L. West, and L. F. Bosart, 2009: Discrete frontal propagation over the Sierra–Cascade Mountains and Intermountain West. *Mon. Wea. Rev.*, **137**, 2000–2020, https://doi.org/10.1175/2008MWR2811.1.

Wallace, J. M., and P. V. Hobbs, 1977: *Atmospheric Science: An Introductory Survey*. Academic Press, 467 pp.

West, G. L., and W. J. Steenburgh, 2010: Life cycle and mesoscale frontal structure of an Intermountain cyclone. *Mon. Wea. Rev.*, **138**, 2528–2545, https://doi.org/10.1175/2010MWR3274.1.

——, and ——, 2011: Influences of the Sierra Nevada on Intermountain cold-front evolution. *Mon. Wea. Rev.*, **139**, 3184–3207, https://doi.org/10.1175/MWR-D-10-05076.1.

Williams, P., Jr., 1969: Station descriptions of local effects on synoptic weather patterns. U.S. Weather Bureau Western Region, Tech. Memo. WBTM WR-5 (revised), 54 pp. [Available from NOAA NWS Western Region Headquarters, 125 S. State Street, Rm. 1311, Salt Lake City, UT 84138-1102.]

——, 1972: Western Region synoptic analysis—Problems and methods. NOAA NWS Western Region Tech. Memo. NWSTM WR-71, 71 pp. [Available from NOAA NWS Western Region Headquarters, 125 S. State Street, Rm. 1311, Salt Lake City, UT 84138-1102.]

Woods, V. S., 1983: Rope cloud over land. *Mon. Wea. Rev.*, **111**, 602–607, https://doi.org/10.1175/1520-0493(1983)111<0602:RCOL>2.0.CO;2.